Prostaglandin PGE2 Receptor EP4 Regulates Microglial Phagocytosis and Increases Susceptibility to Diet-Induced Obesity

Anzela Niraula,[1,2] Rachael D. Fasnacht,[1,2] Kelly M. Ness,[1,2] Jeremy M. Frey,[1,2] Sophia A. Cuschieri,[1,2] Mauricio D. Dorfman,[1,2] and Joshua P. Thaler[1,2]

Diabetes 2023;72:233–244 | https://doi.org/10.2337/db21-1072

In rodents, susceptibility to diet-induced obesity requires microglial activation, but the molecular components of this pathway remain incompletely defined. Prostaglandin PGE2 levels increase in the mediobasal hypothalamus during high-fat-diet (HFD) feeding, and the PGE2 receptor EP4 regulates microglial activation state and phagocytic activity, suggesting a potential role for microglial EP4 signaling in obesity pathogenesis. To test the role of microglial EP4 in energy balance regulation, we analyzed the metabolic phenotype in a microglia-specific EP4 knockout (MG-EP4 KO) mouse model. Microglial EP4 deletion markedly reduced weight gain and food intake in response to HFD feeding. Corresponding with this lean phenotype, insulin sensitivity was also improved in HFD-fed MG-EP4 KO mice, though glucose tolerance remained surprisingly unaffected. Mechanistically, EP4-deficient microglia showed an attenuated phagocytic state marked by reduced CD68 expression and fewer contacts with pro-opiomelanocortin (POMC) neuron processes. These cellular changes observed in the MG-EP4 KO mice corresponded with an increased density of POMC neurites extending into the paraventricular nucleus (PVN). These findings reveal that microglial EP4 signaling promotes body weight gain and insulin resistance during HFD feeding. Furthermore, the data suggest that curbing microglial phagocytic function may preserve POMC cytoarchitecture and PVN input to limit overconsumption during diet-induced obesity.

Hypothalamic regulation of energy balance maintains systemic metabolism and body weight homeostasis. A key neurocircuit in the control of food intake and energy balance is the melanocortin system, comprising pro-opiomelanocortin (POMC) neurons and agouti-related peptide neurons in the arcuate nucleus. These mutually inhibitory neurons integrate hormonal and nutritional signals of energy status to calibrate the activity of downstream melanocortin receptor–expressing neurons in the paraventricular nucleus (PVN), thereby controlling sympathetic tone and consummatory drive (1). POMC neurons, in particular, operate over long time frames to limit weight gain by reducing food intake and increasing energy expenditure, and dysfunction in this neuronal subset is thought to be a critical component of obesity pathogenesis (2).

High-fat-diet (HFD) feeding triggers an inflammatory response marked by gliosis in the arcuate nucleus. Under homeostatic conditions, microglia exhibit a ramified morphology with long processes constantly surveilling the brain microenvironment. However, following perturbations, such as HFD, these cells undergo rapid morphological changes marked by a more ameboid-shaped cell body with thicker processes (3). Importantly, this structural remodeling is indicative of cellular activation, frequently characterized by production of cytokines and immune mediators, such as interleukin-1β (IL-1β) and tumor necrosis factor-α (TNF-α), as well as increased phagocytic activity (4,5). These microglial changes, collectively referred to as gliosis, contribute to susceptibility to diet-induced obesity (DIO) because pharmacological depletion of microglia or genetic disruption of their nuclear factor κ-light-chain-enhancer of activated B cells (NF-κB) signaling pathway reduces food intake and weight gain

[1]UW Medicine Diabetes Institute, University of Washington, Seattle, WA
[2]Department of Medicine, University of Washington, Seattle, WA
Corresponding author: Joshua P. Thaler, jpthaler@uw.edu

Received 23 November 2021 and accepted 23 October 2022
This article contains supplementary material online at https://doi.org/10.2337/figshare.21390963.

during HFD feeding (3,6). However, the downstream mechanisms triggered by HFD feeding to alter microglial activity remain poorly characterized.

Prostaglandins are signaling lipids derived from arachidonic acid that are present throughout the body and perform an array of functions in health and disease (7). The prostaglandin PGE2 is a key inflammatory mediator that regulates apoptosis, angiogenesis, and cell proliferation but is also implicated in diseases such as stroke, neurodegenerative conditions, and cancer (7,8). Under physiologic conditions, PGE2 originates from many cellular sources in the brain, including tanycytes and astrocytes, as well as from neurons themselves (9,10). Similarly, inflammatory stimuli trigger PGE2 release from diverse cell types, including vascular endothelium (important for the fever response), microglia, and others (11). PGE2 signals through four G-protein–coupled receptors (EP1–4), the downstream effects of which vary across tissues, cell types, and conditions (8). While the role of PGE2 in DIO is unclear, HFD-fed mice have elevated levels of the prostaglandin PGE2 in the arcuate nucleus (12), which could modulate microglial activity through the EP receptors. EP4 is highly expressed in microglia and generally serves to constrain the microglial response to inflammatory stimuli, such as lipopolysaccharide, and promote engulfment of β-amyloid plaques in rodent models of Alzheimer disease (13,14). However, the effect of EP4 signaling can vary based on context and timing. For example, in experimental autoimmune encephalomyelitis, a rodent model of multiple sclerosis, EP4 signaling promotes the development of pathology in early stages of disease but reduces severity at later time points (15). Since EP4-null mice develop a lipodystrophic phenotype with a shortened life span (16), it is critical to study EP4 function using cell-specific methods to determine its precise role in metabolic homeostasis.

In the current study, we delineated the role of microglial EP4 signaling in energy balance and glucose homeostasis. Microglial EP4 deletion markedly reduced weight gain during HFD feeding as a result of lower energy intake with no effect on chow-fed mice. Notably, mice with EP4-deficient microglia showed evidence of less microglial phagocytic activity, which was associated with fewer microglia-neuron cell-cell contacts and greater POMC neuron fiber density in the PVN, suggesting their lean phenotype results from preservation of the melanocortin system during DIO.

RESEARCH DESIGN AND METHODS

Mice

Microglia-specific EP4 knockout (MG-EP4 KO) mice were generated by crossing the CX3CR1$^{(CreERT2/+)}$ [B6.129P2(Cg)-Cx3cr1$^{tm2.1(cre/ERT2)Litt}$/WganJ, stock no. 021160; The Jackson Laboratory] line with the Ptger4$^{fl/fl}$ line. Mice were injected at 6 weeks of age with two doses of tamoxifen 4 mg s.c. prepared in corn oil (T5648; Sigma-Aldrich) 48 h apart. Following a 4-week period to allow replenishment of peripheral myeloid cells (17), mice were single housed and placed on a 60% kcal HFD (D12492i; Research Diets) or chow standard diet (5053; LabDiet). All mice had ad libitum access to food and water, except during fasting experiments, and were housed in a temperature-controlled room with a 14-h/10-h light/dark cycle. All experiments and procedures were performed in accordance with the National Institutes of Health Guidelines for Care and Use of Animals and were approved by the institutional animal care and use committee of the University of Washington.

Microglial Isolation

At 3 weeks of HFD, brain microglia were isolated on Percoll gradients, followed by sorting (FACSAria II; Becton Dickinson) using PerCP-conjugated anti-CD11b antibody (cat. no. 550993; BD Pharminogen) into RNA lysis buffer (QIAGEN) for quantitative PCR (qPCR) analysis. Brains from chow-fed mice were isolated and processed by magnetic-activated cell sorting with anti-CD11b MicroBeads (130-049-601; Miltenyi Biotec). CD11b^{+} and CD11b^{-} cells were stained with DAPI, placed on glass slides, and coverslipped, and EYFP was visualized using an epifluorescence microscope (Eclipse E600; Nikon) with a hoisted Nikon camera.

Gene Expression Analysis

FACS microglia and hypothalamus blocks were stored at −80°C until RNA extraction. RNA isolation was performed following the manufacturer's instructions using the QIAGEN RNeasy Micro Kit and RNeasy Mini Kit for FACS microglia and whole hypothalamus, respectively. cDNA samples were generated using the High-Capacity cDNA Reverse Transcription Kit (Thermo Fisher Scientific), and real-time qPCR was performed on the 7900HT system (Applied Biosystems) using SYBR Green Mix. Data were analyzed using the sequence detection software SDS 2.2 (Applied Biosystems). Gene expression levels were measured relative to 18S, and fold change was determined using the ΔΔCt method.

Body Composition and Indirect Calorimetry

Body composition analysis was performed using EchoMRI. Indirect calorimetry was performed at the University of Washington Nutrition Obesity Research Center facility using metabolic cages (Promethion; Sable Systems). Respiratory quotient was calculated as a ratio of CO_2 production to O_2 consumption. Continuous data were binned by hour for analysis and presentation. Calorimetry data were adjusted for body composition differences using ANCOVA.

Intraperitoneal Glucose Tolerance Test and Intraperitoneal Insulin Tolerance Test

Following a 4-h food withdrawal period, mice were injected with a bolus of glucose (2 g/kg i.p., 30% dextrose prepared in saline) or insulin (0.9 units/kg i.p., Humulin prepared in saline), respectively, with tail blood glucose measured using a glucometer (FreeStyle Freedom Lite).

For insulin tolerance test data, glucose was normalized to the baseline value (time 0) for each mouse.

Insulin and Leptin ELISAs

Plasma samples were collected at baseline (nonfasting) or following a 16-h overnight fast. Insulin and leptin ELISAs were performed following the manufacturer's instructions (cat. nos. 90080 and 90030; Crystal Chem).

Intracerebroventricular Administration of EP4 Agonist

Surgical implantation of steel guide cannulas (ALZET; DURECT Corp.) into the lateral ventricle (coordinates: x = 1.3 mm, y = −0.7 mm, z = −1.3 mm) was performed under isoflurane with 2 weeks postoperative recovery. EP4 agonist L-902688 (25 nmol; Cayman Chemicals) or DMSO vehicle was administered centrally (1 μL i.c.v., two doses 3 days apart), with PBS and 4% paraformaldehyde perfusion for immunofluorescence performed 2 h after the second dose.

Immunofluorescent Labeling and Microscopy

Twenty-five-micrometer free-floating coronal sections collected on a freezing stage microtome (Leica SM2010R) were blocked using 5% normal donkey serum (Jackson ImmunoResearch), followed by overnight incubation with the primary antibodies rabbit anti-Iba-1 (1:1,000; Wako), goat anti-Iba-1 (1:1,000; Abcam), rat anti-CD68 (1:1,000; Bio-Rad), rabbit anti-POMC (1:4,000; Phoenix Pharmaceuticals), rabbit anti–β-endorphin (1:5,000; Phoenix Pharmaceuticals), and sheep anti–α-melanocyte–stimulating hormone (α-MSH) (1:10,000; Sigma Millipore) and secondary antibodies donkey anti-rabbit Alexa Fluor 488 (1:500; Thermo Fisher Scientific), donkey anti-rat Alexa Fluor 594 (1:500; Thermo Fisher Scientific), donkey anti-rabbit Alexa Fluor 594 (1:500; Thermo Fisher Scientific), and donkey anti-rabbit Alexa Fluor 647 (1:500; Thermo Fisher Scientific). DAPI (1:10,000) was used for nuclear staining. Sections were mounted on slides and coverslipped in the presence of mounting medium (Fluoromount-G; Thermo Fisher Scientific).

For CD68 expression analysis, immunolabeled sections were imaged on a KEYENCE BZ-X800 inverted microscope at 20× (CD68, Iba-1) and analyzed using ImageJ software. A region of interest (ROI) was created delineating the arcuate nucleus region. A uniform threshold for positive labeling of CD68 was determined, and percent $CD68^+$ area was calculated using ImageJ software on the basis of the thresholded target. For $CD68^+$ puncta analysis, particles with an area of 5–10 μm^2 were considered positive. Counts were manually obtained in a blinded fashion for six microglia from two arcuate nucleus sections each per mouse, and data are presented as overall per-mouse averages. POMC neuron projections were imaged at 10×, followed by thresholding and densitometry within the ROI (PVN approximately −0.8 mm bregma) as described above for CD68 area analysis.

For microglia-POMC overlap analysis, immunolabeled sections were imaged at 40× using the Leica SP8 X microscope at the W.M. Keck Microscopy Center, University of Washington. Arcuate nucleus and PVN imaging were done on separate days. Confocal Z-stack images were imported into Imaris software (Bitplane) and subjected to automated three-dimensional (3D) rendering using the Surface module on the Iba-1 channel and the POMC channel. The mask channel option was used to delineate POMC soma and neurites. The volume of POMC signal within −2 μm and 0 μm distance from the Iba-1 (microglia) signal was calculated by the Imaris software to determine POMC soma or neurite internalization by microglia. All sample imaging and analyses for a given brain region were performed blinded in randomized order on the same day using the same settings.

For microglia-β-endorphin apposition analysis, samples were visualized using a KEYENCE BZ-X800 inverted microscope. Images were captured at 60× using the sectioning feature to generate a Z-stack (1-μm slice, 30 slices per stack) and processed using the maximum projection intensity feature. Microglial contact with β-endorphin puncta and soma were manually counted per image in a randomized and blinded manner.

Microglial Sholl and Morphology Analysis

Sholl analysis was performed using the Sholl plugin in Fiji (ImageJ Fiji; National Institutes of Health). Briefly, images were transformed into binary and thresholded to clearly visualize microglia and processes. Two microglia per image (field of view) in two images per mouse were analyzed. Each cropped microglia was reconstructed via tracing using the Simple Neurite Tracer plugin in Fiji. A fixed ROI was drawn at the soma of the reconstructed microglia. The start radius was set at 0.05 arbitrary units and end radius at 4 arbitrary units, with step size of 0.2. Number of intersections were automatically generated by the software. Data were averaged across microglia, and an area under the curve was calculated for each mouse. Soma size, circularity, and Feret length were calculated using the ROI feature in Fiji.

In Vitro Phagocytosis Assay

BV2 cells (a gift from Dr. Suman Jayadev, University of Washington) were cultured and passed three times prior to experiment. Cells were plated onto a 12-well plate (50,000 cells per well) and incubated in DMEM supplemented with 5% FBS and 1% penicillin/streptomycin at 37°C in 5% CO_2 overnight. Upon reaching confluency, cells were serum starved 24 h prior to the experiment. On the day of the experiment, cells were treated with varying concentrations of the EP4 agonist L-902688 for 1 h, followed by incubation with fluorescent-tagged carboxylate-coated 2-μm-sized latex beads (L3030; Sigma-Aldrich) for 3 h. Cells were detached from the wells with light trypsinization, followed by washes and flow analysis (FACSCanto; Becton Dickinson). DAPI was used to exclude dead cells. Cells positive for phycoerythrin were gated and quantified as a percentage of total viable cells.

Statistics

Groupwise comparisons used unpaired two-tailed Student *t* tests performed with GraphPad Prism 9.0.2. Body weight gain and cumulative food intake data were analyzed using a two-way ANOVA, and post hoc tests were performed using Šidák test to correct for multiple comparisons. Indirect calorimetry data for heat production were analyzed using ANCOVA, with body mass as covariate. Results are presented as mean ± SEM. $P < 0.05$ was considered statistically significant.

Data and Resource Availability

The data sets and resources generated and/or analyzed during the current study are available from the corresponding author upon reasonable request.

RESULTS

Microglial EP4 Deletion Reduced Susceptibility to DIO

A recent study reported an increase in prostaglandin PGE2 levels in the arcuate nucleus following HFD feeding (12). Interestingly, we found a near-significant increase in expression of the receptor EP4 (encoded by the gene *Ptger4*) in isolated microglia but not whole hypothalamus from 1-week HFD-fed mice (Supplementary Fig. 1*A* and *B*), suggesting a potential role for EP4 in diet modulation of microglial function. Activation of EP4, a Gs-protein–coupled receptor, triggers the cAMP pathway. HFD significantly reduced *Egr1* (a downstream target of the cAMP response element–binding protein [CREB]) expression in isolated hypothalamic microglia (Supplementary Fig. 1*C*), implicating EP4 in the microglial response to HFD feeding. To explore this possibility further, we generated $CX3CR1^{CreERT2(+/-)\ IRES\ EYFP}$::$Ptger4^{fl/fl}$ mice (MG-EP4 KO) and $CX3CR1^{CreERT2(-/-)}$::$Ptger4^{fl/fl}$ littermate controls (wild type [WT]), which are predicted to develop EP4 deficiency in microglia upon tamoxifen treatment. As expected, tamoxifen treatment led to a significant reduction (∼79%) in microglial *Ptger4* expression in the MG-EP4 KO mice compared with WT littermates (Supplementary Fig. 2*A*). To confirm the cellular specificity of the EP4 KO, we isolated $CD11b^+$ cells (central nervous system [CNS] microglia/myeloid) and $CD11b^-$ cells (neurons and other glia) from WT and MG-EP4 KO mice using magnetic-activated cell sorting. Given that *EYFP* and *CreERT2* are cotranscribed from a bicistronic mRNA cassette knocked into the *Cx3cr1* locus, EYFP fluorescence serves as a faithful marker of *Cre* expression. We found EYFP only in $CD11b^+$ cells and not in any population of $CD11b^-$ cells (Supplementary Fig. 2*B* and *C*), indicating that EP4 deletion occurred exclusively in the CNS myeloid compartment of the MG-EP4 KO mice. Next, we examined the effects of Cre-mediated EP4 deletion on microglial morphology following at least 6 weeks after tamoxifen administration. Sholl analysis revealed that microglia from MG-EP4 KO mice had a more ramified structure than microglia from WT mice, as indicated by a greater number of intersections with the Sholl radii (Supplementary Fig. 2*D* and *E*). Greater ramifications usually suggest a more quiescent microglial phenotype (18,19), but we found that microglial expression of CD68, a lysosomal marker expressed in phagocytically active cells, was equally low in MG-EP4 KO and WT mice at the protein (Supplementary Fig. 2*F* and *G*) and mRNA (Supplementary Fig. 2*H*) levels. Thus, under baseline conditions when microglia are already in a quiescent state, EP4 deletion has little impact on their function. Corresponding with these findings, MG-EP4 KO and WT mice fed standard chow did not differ in body weight (Supplementary Fig. 2*I*), glucose tolerance (Supplementary Fig. 2*J*), or insulin tolerance (Supplementary Fig. 2*K*), indicating that microglial EP4 signaling is dispensable for energy balance under normal physiologic conditions as expected when hypothalamic PGE2 levels are low (12).

EP4 deletion caused microglia to adopt a more quiescent morphological profile, but this did not impact systemic physiology under basal conditions. However, this morphologic phenotype raised the possibility that EP4-deficient microglia may be more resistant to the activating effects of HFD feeding observed in male mice (3). Accordingly, we hypothesized that male MG-EP4 KO mice would have reduced susceptibility to DIO. Indeed, MG-EP4 KO mice had a marked protection from HFD-induced weight gain (Fig. 1*A* and *B*) and fat mass gain (Fig. 1*C*) compared with the WT mice. Though lean mass was modestly reduced as well (Fig. 1*C*), lower plasma leptin levels in KO mice (Fig. 1*D*) indicated a strong effect of microglial EP4 deletion on the regulation of adiposity. Tracking of food intake over the course of 105 days of HFD feeding revealed significantly lower cumulative food intake in the MG-EP4 KO animals (Fig. 1*E*). Female MG-EP4 KO mice showed no differences in food intake or body weight compared with controls (data not shown), which was expected based on the known resistance of female mice to HFD-induced microglial activation and weight gain (20).

Examining food intake in calorimetry cages revealed that male MG-EP4 KO mice had consumed less of the HFD in both dark and light cycles (Fig. 1*F* and *G*), resulting in reduced total daily intake (Fig. 1*H*). Surprisingly, body weight–normalized energy expenditure was also lower in MG-EP4 KO mice (Fig. 1*I–K*), suggesting a compensatory metabolic mechanism to offset hypophagia. However, with the respiratory quotient closer to 0.7 (the level indicative of fat utilization) in KO mice (Fig. 1*L* and *M*), this adaptation is apparently inadequate, resulting in consistent body weight differences between genotypes. Overall, these results indicate that microglial EP4 signaling promotes HFD-induced hyperphagia and susceptibility to DIO.

Microglial EP4 Deletion Improved Insulin Tolerance on HFD

Given the lean phenotype induced by microglial EP4 deletion, we hypothesized that obesity-associated glucose intolerance would be improved in MG-EP4 KO mice. However,

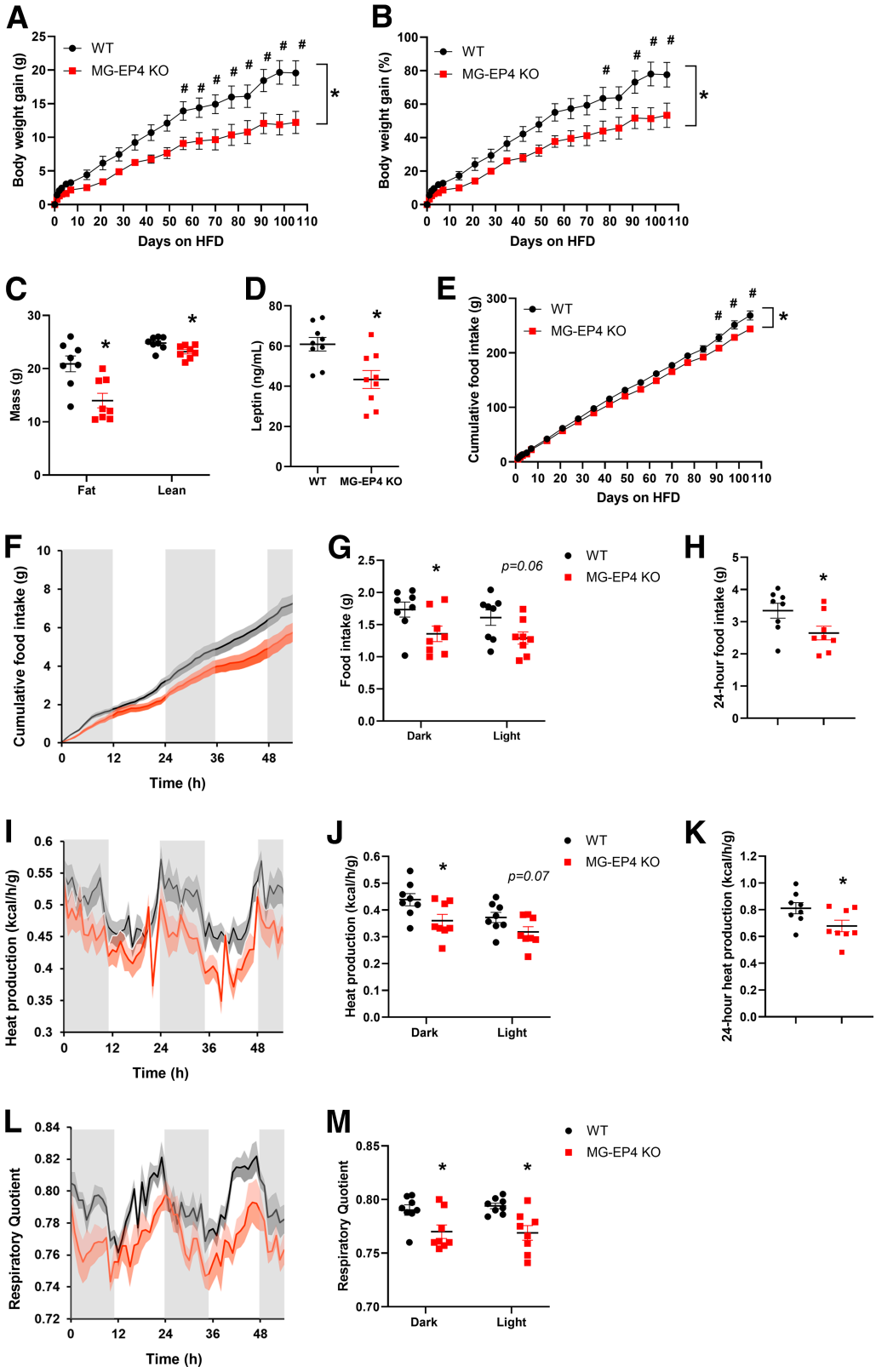

Figure 1—Microglial EP4 deletion reduced susceptibility to DIO. *A–E*: Absolute body weight gain (*A*), percentage body weight gain (*B*), fat mass and lean mass (*C*), plasma leptin (*D*), and cumulative food intake (*E*) in male WT and MG-EP4 KO mice fed an HFD for 16 weeks (n = 8–9). *F–H*: Continuous measurements of cumulative food intake (*F*), binned dark cycle and light cycle food intake (*G*), and total 24-h food intake (*H*). *I–K*: Heat production traces (*I*), quantification of dark cycle and light cycle (*J*), and total heat production (*K*). *L* and *M*: Respiratory quotient traces (*L*) and quantification of dark cycle and light cycle respiratory quotient (*M*) following 16 weeks of HFD (n = 8). Body weight gain and cumulative food intake data analyzed by two-way ANOVA with Šidák test. Data in *I–K* analyzed by ANCOVA with body mass as covariate. Data are mean ± SEM. *$P < 0.05$ for genotype × time interaction in ANOVA; #$P < 0.05$ for post hoc analysis.

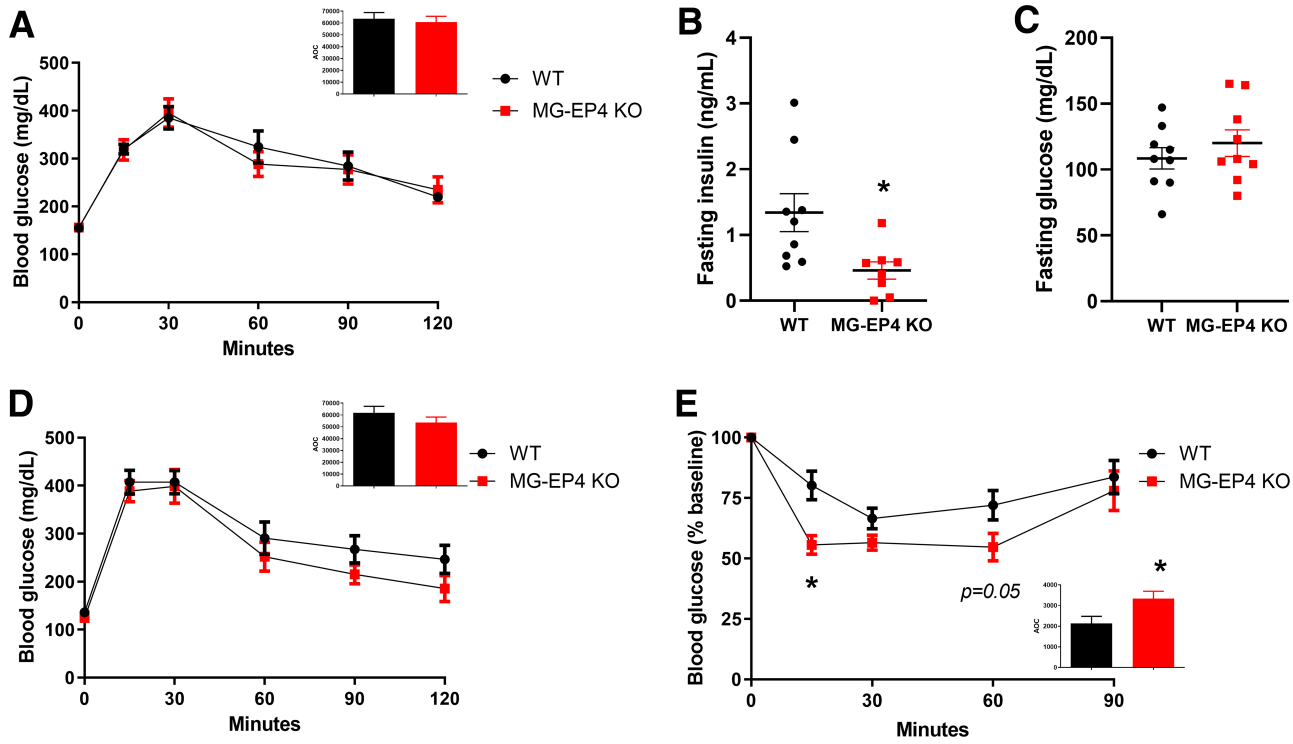

Figure 2—Microglial EP4 deletion improved insulin tolerance during HFD. *A*: Intraperitoneal glucose tolerance test (2 g/kg i.p.) and area under curve (AUC) analysis (inset) from male WT and MG-EP4 KO mice following 12 weeks of HFD feeding ($n = 9$). *B* and *C*: Fasting plasma insulin and glucose levels at 12 weeks of HFD. *D*: Intraperitoneal glucose tolerance test with AUC (inset) at 22 weeks of HFD. *E*: Insulin tolerance test (0.9 units/kg) with area over curve (AOC) (inset) at 23 weeks of HFD ($n = 9$). Data are mean ± SEM. *$P < 0.05$ by Student *t* test.

no differences in glucose tolerance between genotypes were observed at 12 weeks of HFD (Fig. 2*A*). Instead, MG-EP4 KO mice showed lower fasting plasma insulin (Fig. 2*B*) with no difference in fasting glucose (Fig. 2*C*), suggesting increased insulin sensitivity. Similar results were obtained at 22–23 weeks of HFD, with equivalent glucose tolerance (Fig. 2*D*) but improved insulin tolerance in MG-EP4 KO mice compared with WT controls (Fig. 2*E*). Overall, the unaltered glucose tolerance of MG-EP4 KO mice suggests that their insulin sensitivity likely improved as an indirect consequence of reduced adiposity rather than a direct effect on glucose homeostasis.

Microglial EP4 Deletion Reversed Key HFD-Induced Alterations to Microglial Attributes

Our findings demonstrate a positive association between microglial EP4 deletion and reduced susceptibility to weight gain and insulin resistance during HFD feeding. To begin to elucidate the mechanisms underlying this phenotype, we examined microglial properties that are altered during HFD exposure. Morphological assessment of microglia using Sholl analysis following 3 weeks of HFD revealed that MG-EP4 KO mice had more intersections of arcuate nucleus microglia processes with Sholl radii than WT controls, indicating a more ramified structure of EP4-deficient microglia (Fig. 3*A* and *B*). MG-EP4 KO microglia also had larger cell somas (Fig. 3*C*), lower circularity indices (Fig. 3*D*), and longer Feret lengths (i.e., distance between the two farthest points of the cell soma) (Fig. 3*E*). Taken together, these cytological features suggest that EP4 deficiency renders microglia less susceptible to HFD-mediated activation.

On the basis of the morphological analysis above, we predicted that MG-EP4 KO microglia would have reduced inflammatory gene expression consistent with a less activated profile. Unexpectedly, however, microglial *Tnfα* and *Il1β* mRNA levels did not differ between genotypes after 3 weeks of HFD feeding (Fig. 3*F*). Instead, expression of the phagocytosis gene *Cd68* was significantly reduced in the MG-EP4 KO microglia compared with the WT (Fig. 3*F*). Examining tissue sections of the mediobasal hypothalamus, we observed that CD68 immunoreactivity was diminished in the arcuate nucleus in the MG-EP4 KO mice (percent area) (Fig. 3*G* and *H*). As a lysosomal membrane-associated glycoprotein (21), CD68 produces a punctate staining pattern under immunofluorescence (Fig. 3*G*, inset). Quantification of high-magnification images revealed fewer $CD68^+$ puncta localized in MG-EP4 KO microglia (Fig. 3*I*). Notably, the degree of change in microglial CD68 puncta was on the same order as that observed in models of Huntington disease (22), maternal immune activation (23), and Alzheimer disease (21).

Reduced CD68 in KO microglia suggests that microglial phagocytosis is regulated by EP4 signaling. To test this hypothesis in vitro, we treated the murine microglial cell line BV2 with the selective EP4 agonist L-902688, and

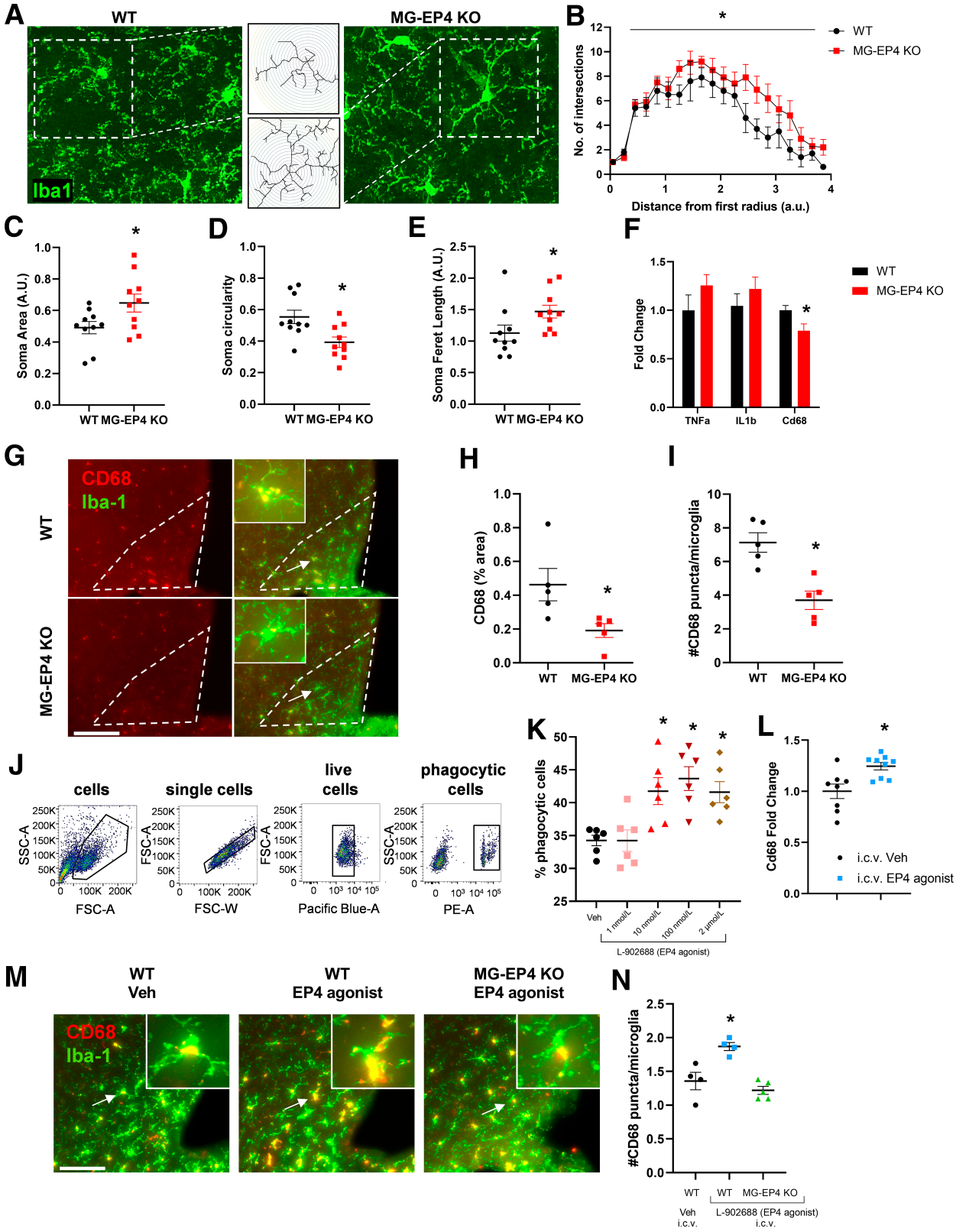

Figure 3—Microglial EP4 deletion reversed key HFD-induced alterations to microglial attributes. *A*: Representative maximum intensity projection images of fluorescently labeled Iba-1$^+$ microglia from WT and MG-EP4 KO mice following 3 weeks of HFD. Insets represent reconstructed cells (shown in the middle panel [top, WT; bottom, MG-EP4 KO]). *B*: Area under the curve comparison between WT and MG-EP4 KO mice following Sholl analysis of microglial process intersections. *C–E*: Cell soma area, circularity, and Feret length. Data points represent two sections per mouse (n = 5). *F*: Real-time qPCR measurements of genes from FACS microglia following 3 weeks of HFD (n = 8–10). *G*: Representative images of CD68 and Iba-1 immunofluorescence labeling from WT and MG-EP4 KO brains following

measured phagocytosis of fluorescently labeled carboxylate-coated latex beads using flow cytometry. EP4 agonist treatment increased the percentage of phagocytic cells at concentrations >1 nmol/L (Fig. 3*J* and *K*). Central administration of the EP4 agonist L-902688 (25 nmol i.c.v.) in WT mice increased *Cd68* mRNA levels in the hypothalamus (Fig. 3*L*). Similarly, intracerebroventricular EP4 agonist administration increased the number of $CD68^+$ puncta in the microglia of the WT group but not in the MG-EP4 KO group (Fig. 3*M* and *N*). Together, these data demonstrate that EP4 receptor activation triggers the microglial phagocytic response in vivo and in vitro, providing a counterpoint for the more homeostatic (nonphagocytic) microglial phenotype observed with EP4 deficiency.

Microglial EP4 Deficiency Preserved POMC Neuron Projections to the PVN During HFD Feeding

Previous studies have demonstrated that HFD feeding triggers alterations to POMC neurons that contribute to obesity pathogenesis, including cell-cell contact with activated microglia and disruption of downstream melanocortin signaling (24,25). Here, we first examined whether and how microglial contacts with POMC neurons are altered during HFD feeding. We performed immunofluorescent labeling and confocal imaging of the arcuate nucleus microglia and POMC neurons in a cohort of chow- and HFD-fed mice, followed by automated 3D reconstruction of the confocal Z-stacks using Imaris analysis. Compared with chow conditions, 1 week of HFD feeding significantly increased the percentage of overlap between microglia and POMC puncta (Supplementary Fig. 3*A*–*G* and rendered in 3D in Supplementary Video 1), demonstrating greater internalization of POMC processes by microglia during HFD feeding. As expected, there was no difference between chow and HFD in microglial overlap with POMC soma, suggesting that POMC neurons remain viable during HFD feeding (Supplementary Fig. 3*H*). Indeed, there was no difference in the number of POMC cells, though microglial volume was increased in the HFD group (Supplementary Fig. 3*I* and *J*). Consistent with the immunohistochemical findings, HFD feeding increased hypothalamic expression of key genes indicative of phagocytosis (*Cd68*, *Apoe*, *MerTK*, *Itgam*) (Supplementary Fig. 3*K*–*N*). Taken together, the microglial phagocytic response to HFD is characterized by internalization of POMC processes, likely altering melanocortin signaling and POMC projections to distal targets (see below).

Given the attenuated phagocytic profile of EP4-deficient microglia in HFD-fed mice, we hypothesized that microglial internalization of POMC processes would be reduced during DIO in the MG-EP4 KO mice compared with the WT. We again used Imaris analysis to assess microglial overlap with POMC neurons. As predicted, there was a significant reduction in percent overlap between POMC puncta and microglia (WT group in Fig. 4*A* and *C* and MG-EP4 KO group in Fig. 4*B* and *E*) but not POMC soma and microglia (Fig. 4*D* and *F*) in the MG-EP4 KO mice compared with WT (Fig. 4*G* and *H*). The overall microglial volume and the number of POMC cells did not differ by genotype (Supplementary Fig. 4*A* and *B*). The reduced microglia-POMC puncta overlap was also evident in samples where staining for the POMC cleavage product β-endorphin was used as a proxy to visualize POMC neurons (Supplementary Fig. 4*C*–*F*). Corresponding with findings from POMC immunolabeling (Fig. 4), there was no difference in the number of microglia (Supplementary Fig. 4*G*) or β-endorphin–positive cells (Supplementary Fig. 4*H*) between the WT and MG-EP4 KO groups. Overall, these findings indicate that HFD-induced microglial internalization of POMC processes is reduced in MG-EP4 KO mice.

One of the primary targets of POMC neurons is the PVN melanocortin receptor 3/4–expressing neurons, which provide a strong anorexigenic signal in response to agonism by the POMC cleavage product α-MSH (1). This pathway is rapidly disrupted during HFD feeding through an unknown mechanism. Consistent with the reduced microglia-POMC overlap and phagocytic profile of EP4-deficient microglia, $POMC^+$ area (Fig. 4*I* and *J*) and POMC intensity (Fig. 4*K*) in the PVN were markedly higher in HFD-fed MG-EP4 KO mice. Correspondingly, we also observed greater $\alpha\text{-MSH}^+$ (Fig. 4*L* and *M*) and β-endorphin area (Supplementary Fig. 4*I* and *J*) and α-MSH intensity (Fig. 4*N*) in the HFD-fed MG-EP4 KO mice. Together, these findings demonstrate that microglial EP4 deletion leads to greater preservation of POMC projections during HFD feeding, a possible mechanism to explain their reduced susceptibility to DIO.

Unlike in the arcuate nucleus, the percentage of microglia-POMC puncta overlap in the PVN did not differ between the MG-EP4 KO mice and WT mice (Supplementary Fig. 5*A*–*E*), indicating that microglial internalization of POMC projections occurred primarily in the arcuate nucleus. Similar to the arcuate nucleus, microglia volume in the PVN did not differ

5 weeks of HFD. Arrows represent $CD68^+$ microglia from the mediobasal hypothalamus also depicted in the insets. Scale bar = 80 μm; inset magnification ×80. *H* and *I*: Quantification of CD68 percent area and number of $CD68^+$ puncta per microglia (n = 4–5). *J*: Representative flow cytometry plots of BV2 cells treated for 3 h with 2-μm phycoerythrin-coated latex beads in the presence of various concentrations of the EP4 agonist (L-902688). *K*: Bead-positive cells out of total live cells quantified as percentage of phagocytic cells (n = 3 from two technical replicates). *L*: *Cd68* mRNA levels in the hypothalamus 1 h after intracerebroventricular administration of the EP4 agonist L-902688 (25 nmol) or vehicle in WT mice (n = 9). *M*: Representative images of CD68 and Iba-1 immunofluorescence in the mediobasal hypothalamus following intracerebroventricular administration of L-902688 (25 nmol) or vehicle in chow-fed WT and MG-EP4 KO mice. Arrows represent $CD68^+$ microglia also depicted in the insets. Scale bar = 80 μm; inset magnification ×80. *N*: Quantification of $CD68^+$ puncta per microglia (n = 4–5). Data are mean ± SEM. Data analyzed by one-way ANOVA with Tukey test for multiple comparisons. $^*P < 0.05$ by Student t test. A.U., arbitrary unit, FSC-A, forward scatter area; FSC-W, forward scatter width; PE-A, phycoerythrin area; SSC-A, side scatter area; Veh, vehicle.

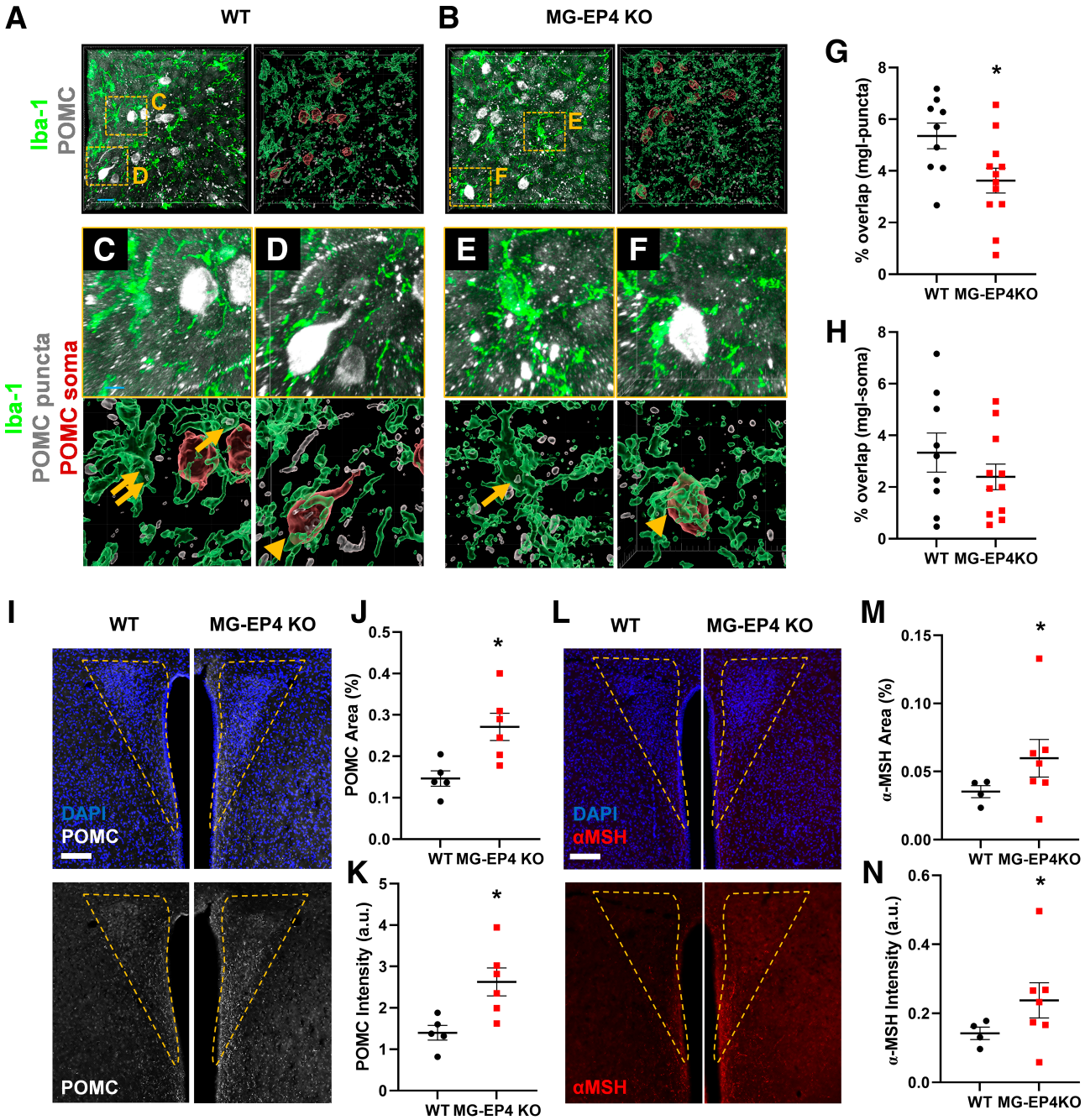

Figure 4—Microglial EP4 deficiency preserved POMC neuron projections to the PVN during HFD feeding. *A* and *B*: Representative images (left) and Imaris 3D rendering (right) of POMC neurons (puncta, gray; soma, red) and Iba-1$^+$ microglia (green) in the arcuate nucleus of WT (*A*) and MG-EP4 KO (*B*) mice following 3 weeks of HFD (scale bar = 20 μm). *C–F*: Insets (top) and Imaris 3D rendering (bottom) from *A* and *B*. Microglial (green) overlap with POMC puncta (gray) represented in *C* and *E*. Microglial (green) overlap with POMC soma (red) represented in *D* and *F* (scale bar = 5 μm). *G* and *H*: Percentage overlap between microglia and POMC puncta (*G*) and microglia and POMC soma (*H*). Data points represent two sections per mouse (n = 5–7). *I–K*: Representative images (scale bar = 100 μm) (*I*), quantification of POMC percent area (*J*), and POMC intensity (*K*) in the PVN (n = 5–7). *L–N*: Representative images (scale bar = 100 μm) (*L*) and quantification (*M*) of α-MSH percent area and α-MSH intensity (*N*) in the PVN (n = 5–7). Data are mean ± SEM. *$P < 0.05$ by Student t test. a.u., arbitrary unit; mgl, microglia.

between the WT and the MG-EP4 KO mice (Supplementary Fig. 5*F*). POMC is a precursor polypeptide enzymatically cleaved into multiple peptides; therefore, we next assessed whether MG-EP4 KO mice on an HFD have altered levels of POMC processing enzymes or other appetite-regulating neuropeptides compared with the WT. Hypothalamic expression of the enzymes *Cpe*, *Pam*, *Pcsk1*, and *Pcsk2* and neuropeptides agouti-related peptide (*Agrp*), orexin (*Hcrt*), and *Pomc* did not differ between the MG-EP4 KO mice and the WT mice (Supplementary Fig. 5*G* and *H*), indicating that

altered POMC processing or neuropeptide synthesis do not contribute to greater POMC projections in the MG-EP4 KO mice during HFD feeding. Together, these data support a model in which the absence of EP4 limits HFD-induced activation of microglial phagocytosis, thereby preserving POMC projections to the PVN and reducing susceptibility to DIO.

DISCUSSION

Microglial activation is both necessary and sufficient to promote weight gain and hyperphagia in response to HFD feeding (6,25), but the specific drivers of this response have not been fully identified. Here, we present evidence that expression of the PGE2 receptor EP4 by microglia is critical for susceptibility to DIO. Specifically, microglial EP4 deficiency confers protection from HFD-induced hyperphagia, weight gain, and insulin resistance, while being dispensable for physiological body weight regulation. At the cellular level, these metabolic improvements correspond with reduced microglial phagocytic activation by HFD, fewer contacts between microglia and POMC neurons, and greater abundance of POMC projections to the PVN. Together, these data implicate EP4-mediated regulation of microglial phagocytosis as an important modulator of energy homeostasis during DIO via impacts on melanocortin circuit integrity.

A recent study implicated hypothalamic PGE2 in microglial activation and metabolic regulation during DIO. Preventing the increase in ventromedial hypothalamic PGE2 during HFD feeding by targeted knockdown of cPLA2, an enzyme involved in the generation of the prostaglandin precursor molecule arachidonic acid, reversed microgliosis and improved glucose tolerance of the HFD (12). However, arachidonic acid is a precursor for all eicosanoids, including other prostaglandins, prostacyclins, thromboxanes, and leukotrienes, making commonality between the phenotypes of the MG-EP4 KO and cPLA2 KO models unlikely. More relevant is a mouse model with global deletion of the key enzyme for PGE2 synthesis mPGES-1, which showed reduced food intake and weight gain with an HFD (26). In contrast, tanycyte production of PGE2 (a major cellular source under basal conditions) sustains POMC neuronal signaling via lactate supply (9) and is critical for inflammation-induced anorexia (27). Overall, these reports implicate PGE2 signaling in energy balance regulation, although cellular and tissue context are critical, and the mechanisms involved remain elusive.

Among the four receptors for PGE2, EP4 is highly expressed throughout the body and exerts various physiological and pathological roles in inflammatory processes, lipid uptake, and vascular functions (8). Global deletion of EP4 leads to a lipodystrophic phenotype with reduced weight gain, suggesting that the function of EP4 at the systemic level is dominated by its role in adipose tissue (16). EP4 is also the primary PGE2 receptor expressed in macrophages where it has been implicated in atherosclerotic lesions in humans and mice (28,29). Finally, microglia express among the highest levels of EP4 in the mouse and human brain (30,31), but prior studies have largely focused on its role in bacterial challenge and Alzheimer disease. Thus, our study is the first to describe a function for microglial EP4 signaling in obesity pathogenesis, representing an important step forward in elucidating the involvement of CNS prostaglandins in metabolism.

Our finding that microglial EP4 deletion limits food intake and body weight gain during HFD feeding adds to a small, but growing body of literature implicating microgliosis in obesity pathogenesis. Interestingly, two mouse models involving microglial deletion of *Ikkβ* and mitochondrial uncoupling protein 2 (*Ucp2*), respectively, showed a similar level of obesity resistance (~6–7 g less than controls over a 12–18-week HFD) as the MG-EP4 KO mice (6.5 g over a 17-week HFD) (6,25). Conversely, microglial lipoprotein lipase (Lpl)–deficient mice gained excess weight to a similar extent (~7 g) (32). While the metabolic alterations observed in these mouse lines was largely ascribed to reduced hypothalamic inflammation, we provide a novel mechanism for the MG-EP4 KO model based on preservation of POMC neuron-PVN projections during HFD feeding. Similar alterations to the POMC-PVN neurocircuit have been described in the context of aging, intrauterine HFD exposure, and short-term HFD feeding (33–35), suggesting that a common pathway involving structural compromise of the melanocortin system may underlie environmentally induced metabolic dysfunction. While the precise mechanism underlying this vulnerability is unknown, the preserved architecture of the melanocortin neurocircuit during DIO in MG-EP4 KO mice corresponded with fewer phagocytic contacts between microglia and POMC neuron soma and projections at the level of the arcuate nucleus (but not the PVN). As discussed in more detail below, microglial phagocytosis and its impact on neurocircuit integrity represent a novel mechanism for future studies on metabolic physiology and pathology.

During HFD feeding, the levels of inflammatory cytokines, such as IL-1β and TNF-α, as well as markers of phagocytosis, such as the myeloid-specific lysosome-associated glycoprotein CD68, increase together with the onset of gliosis in the arcuate nucleus (3). In MG-EP4 KO mice, there were no changes in inflammatory signaling in DIO, despite previous reports that microglial EP4 signaling helps to resolve inflammation following lipopolysaccharide challenge (13). In contrast, CD68 levels were significantly reduced along with microglia, displaying a less activated phenotype characterized by a homeostatic pattern of more branching of projections and an elongated, less ameboid cell body. Thus, these data support the novel finding that the microglial phagocytic and morphological activation responses are regulated separately from the inflammatory cytokine response in the context of DIO.

A reduced microglial phagocytic state in the absence of EP4 signaling may impact synapse remodeling. As the resident phagocytes of the CNS, microglia are responsible for maintaining synaptic integrity. For example, microglial

engulfment of presynaptic inputs from retinal ganglion cells via the complement pathway is critical in synapse pruning and stabilization (36). Likewise, microglial phagocytosis of apoptotic neurons via receptor tyrosine kinases is key in debris clearance during development and injury (37). Microglia also phagocytose dendritic spines, whole neurons, extracellular matrix components, and myelin debris, all of which may profoundly alter neuronal circuitry and physiological outcomes (37–40). In the context of pathology, aberrant microglial phagocytosis is associated with disruption of neurocircuits or impairment of neuronal function, such as in autism and Alzheimer disease (21,41). In fact, deficiency of microglial EP4 disrupts amyloid phagocytosis, leading to increased plaque accumulation and plaque density in the hippocampus of a mouse model of Alzheimer disease (14). Our current study demonstrates that EP4 deficiency reduces the phagocytic state of microglia, leading to fewer phagocytic contacts between microglia and POMC projections at the level of the arcuate nucleus. In contrast, there were no differences in associations in the PVN. Nevertheless, microglia EP4 deficiency led to preserved POMC projections to the PVN. Overall, this suggests a model by which HFD feeding triggers EP4 activation of microglial phagocytic engulfment of POMC neuronal segments in the arcuate nucleus; the consequent disruption of anterograde communication to terminal fibers in the PVN would cause their retrograde degeneration, leading to a reduction in melanocortin signaling. Follow-up studies will be critical to test this hypothesis and delineate the specific impact of HFD-triggered phagocytosis on hypothalamic circuit remodeling.

In contrast with our study, a previous report using a microglia-specific Lpl deletion model found reduced CD68 expression associated with increased body weight gain on a high-fat, high-sucrose diet (32). One potential explanation for the discrepancy may be a different substrate of phagocytosis in the context of LPL versus EP4. Indeed, microglial Lpl deletion on HFD was associated with fewer POMC neurons (32), while microglial EP4 deletion in the current study did not alter the total number of POMC neurons (nor did loss of UCP2 [25]). Instead, microglial EP4 deletion resulted in reduced internalization of POMC processes, the direct converse of a previous study (from the same authors as the Lpl study), showing that increased microglia-POMC neuron contacts are associated with HFD-induced weight gain (24). The association of these reduced cell-cell contacts with a more intact melanocortin neurocircuit suggests a mechanism linking microglial phagocytosis to the maintenance of POMC neuron function during HFD feeding. Indeed, greater melanocortin fiber density in the PVN has been associated with intact sickness-associated anorexia responses in adult mice (42), while depletion of these projections in mice lacking protein kinase Cλ in POMC neurons results in profound obesity in the context of HFD exposure (43). Given that POMC neurons comprise a heterogeneous population with diverse functional properties, future studies will need to further characterize neuron-microglia appositions in specific POMC (and other neuronal) subpopulations and determine their role in DIO pathogenesis.

In conclusion, microglial EP4 deletion conferred protection from DIO and obesity-associated insulin resistance. EP4 signaling was associated with a phagocytic response to HFD, and abrogation of this pathway suppressed the microglial phagocytic state, yielding fewer microglia-POMC neuron contacts and preserved POMC projections in the PVN. Together, these data implicate PGE2 signaling via EP4 as an important regulator of microglial-POMC neuron interactions during HFD feeding that drives susceptibility to metabolic dysfunction and provide a basis for investigating microglial phagocytosis as a novel target for obesity therapeutics.

Acknowledgments. The authors acknowledge the technical assistance provided by Olivia Santiago at the University of Washington and Kayoko Ogimoto and Jarrell Nelson in the Energy Balance Core of the University of Washington Nutrition Obesity Research Center. The authors thank the members of the Michael Schwartz laboratory for many discussions about the data. The authors also thank Dr. Karin Bornfeldt, University of Washington, for the gift of the Ptger4$^{fl/fl}$ mouse line (line originally generated by Matthew and Richard Breyer, Vanderbilt University). Assistance with metabolic phenotyping was provided by the Nutrition Obesity Research Center (DK035816) and the Diabetes Research Center (DK017047) at the University of Washington.

Funding. This work was supported by National Institute of Diabetes and Digestive and Kidney Diseases grant R01 DK119754 (to J.P.T.) and American Heart Association postdoctoral fellowship 20POST35210291 (to A.N).

Duality of Interest. No potential conflicts of interest relevant to this article were reported.

Author Contributions. A.N. led the project and performed the experiments. A.N. and J.P.T. designed the overall study, analyzed all data, and wrote the manuscript. R.D.F. performed the initial pilot studies. K.M.N., J.M.F., and M.D.D. assisted with mouse physiology studies. S.A.C. assisted with immunohistochemical experiments and analysis. J.P.T. provided supervision of the initial pilot studies, experiments, and data collection. All authors provided input and editing. J.P.T. is the guarantor of this work and, as such, had full access to all the data in the study and takes responsibility of the integrity of the data and the accuracy of the data analysis.

References

1. Yeo GSH, Chao DHM, Siegert AM, et al. The melanocortin pathway and energy homeostasis: from discovery to obesity therapy. Mol Metab 2021;48:101206

2. Horvath TL, Sarman B, García-Cáceres C, et al. Synaptic input organization of the melanocortin system predicts diet-induced hypothalamic reactive gliosis and obesity. Proc Natl Acad Sci U S A 2010;107:14875–14880

3. Thaler JP, Yi CX, Schur EA, et al. Obesity is associated with hypothalamic injury in rodents and humans. J Clin Invest 2012;122:153–162

4. Keren-Shaul H, Spinrad A, Weiner A, et al. A unique microglia type associated with restricting development of Alzheimer's disease. Cell 2017; 169:1276–1290.e17

5. Norden DM, Trojanowski PJ, Villanueva E, Navarro E, Godbout JP. Sequential activation of microglia and astrocyte cytokine expression precedes increased Iba-1 or GFAP immunoreactivity following systemic immune challenge. Glia 2016;64: 300–316

6. Valdearcos M, Douglass JD, Robblee MM, et al. Microglial inflammatory signaling orchestrates the hypothalamic immune response to dietary excess and mediates obesity susceptibility. Cell Metab 2017;26:185–197.e3

7. Smyth EM, Grosser T, Wang M, Yu Y, FitzGerald GA. Prostanoids in health and disease. J Lipid Res 2009;50(Suppl.):S423–S428
8. Hata AN, Breyer RM. Pharmacology and signaling of prostaglandin receptors: multiple roles in inflammation and immune modulation. Pharmacol Ther 2004; 103:147–166
9. Lhomme T, Clasadonte J, Imbernon M, et al. Tanycytic networks mediate energy balance by feeding lactate to glucose-insensitive POMC neurons. J Clin Invest 2021;131:140521
10. Clasadonte J, Poulain P, Hanchate NK, Corfas G, Ojeda SR, Prevot V. Prostaglandin E2 release from astrocytes triggers gonadotropin-releasing hormone (GnRH) neuron firing via EP2 receptor activation. Proc Natl Acad Sci U S A 2011;108:16104–16109
11. Nilsson A, Wilhelms DB, Mirrasekhian E, Jaarola M, Blomqvist A, Engblom D. Inflammation-induced anorexia and fever are elicited by distinct prostaglandin dependent mechanisms, whereas conditioned taste aversion is prostaglandin independent. Brain Behav Immun 2017;61:236–243
12. Lee M-L, Matsunaga H, Sugiura Y, et al. Prostaglandin in the ventromedial hypothalamus regulates peripheral glucose metabolism. Nat Commun 2021; 12:2330
13. Shi J, Johansson J, Woodling NS, Wang Q, Montine TJ, Andreasson K. The prostaglandin E2 E-prostanoid 4 receptor exerts anti-inflammatory effects in brain innate immunity. J Immunol 2010;184:7207–7218
14. Woodling NS, Wang Q, Priyam PG, et al. Suppression of Alzheimer-associated inflammation by microglial prostaglandin-E2 EP4 receptor signaling. J Neurosci 2014;34:5882–5894
15. Esaki Y, Li Y, Sakata D, et al. Dual roles of PGE2-EP4 signaling in mouse experimental autoimmune encephalomyelitis. Proc Natl Acad Sci U S A 2010;107:12233–12238
16. Cai Y, Ying F, Song E, et al. Mice lacking prostaglandin E receptor subtype 4 manifest disrupted lipid metabolism attributable to impaired triglyceride clearance. FASEB J 2015;29:4924–4936
17. Parkhurst CN, Yang G, Ninan I, et al. Microglia promote learning-dependent synapse formation through brain-derived neurotrophic factor. Cell 2013;155:1596–1609
18. Spencer SJ, Basri B, Sominsky L, et al. High-fat diet worsens the impact of aging on microglial function and morphology in a region-specific manner. Neurobiol Aging 2019;74:121–134
19. Soch A, Sominsky L, De Luca SN, Spencer SJ. Obesity after neonatal overfeeding is independent of hypothalamic microgliosis. J Neuroendocrinol 2019;31:e12757
20. Dorfman MD, Krull JE, Douglass JD, et al. Sex differences in microglial CX3CR1 signalling determine obesity susceptibility in mice. Nat Commun 2017;8:14556
21. Hong S, Beja-Glasser VF, Nfonoyim BM, et al. Complement and microglia mediate early synapse loss in Alzheimer mouse models. Science 2016;352:712–716
22. Savage JC, St-Pierre MK, Carrier M, et al. Microglial physiological properties and interactions with synapses are altered at presymptomatic stages in a mouse model of Huntington's disease pathology. J Neuroinflammation 2020;17:98
23. Hui CW, Vecchiarelli HA, Gervais É, et al. Sex differences of microglia and synapses in the hippocampal dentate gyrus of adult mouse offspring exposed to maternal immune activation. Front Cell Neurosci 2020;14: 558181
24. Yi C-X, Walter M, Gao Y, et al. TNFα drives mitochondrial stress in POMC neurons in obesity. Nat Commun 2017;8:15143
25. Kim JD, Yoon NA, Jin S, Diano S. Microglial UCP2 mediates inflammation and obesity induced by high-fat feeding. Cell Metab 2019;30:952–962.e5
26. Pierre C, Guillebaud F, Airault C, et al. Invalidation of microsomal prostaglandin E synthase-1 (mPGES-1) reduces diet-induced low-grade inflammation and adiposity. Front Physiol 2018;9:1358
27. Böttcher M, Müller-Fielitz H, Sundaram SM, et al. NF-κB signaling in tanycytes mediates inflammation-induced anorexia. Mol Metab 2020;39:101022
28. Takayama K, García-Cardena G, Sukhova GK, Comander J, Gimbrone MAJ Jr, Libby P. Prostaglandin E2 suppresses chemokine production in human macrophages through the EP4 receptor. J Biol Chem 2002;277:44147–44154
29. Babaev VR, Chew JD, Ding L, et al. Macrophage EP4 deficiency increases apoptosis and suppresses early atherosclerosis. Cell Metab 2008;8:492–501
30. Zhang Y, Chen K, Sloan SA, et al. An RNA-sequencing transcriptome and splicing database of glia, neurons, and vascular cells of the cerebral cortex. J Neurosci 2014;34:11929–11947
31. Zhang Y, Sloan SA, Clarke LE, et al. Purification and characterization of progenitor and mature human astrocytes reveals transcriptional and functional differences with mouse. Neuron 2016;89:37–53
32. Gao Y, Vidal-Itriago A, Kalsbeek MJ, et al. Lipoprotein lipase maintains microglial innate immunity in obesity. Cell Rep 2017;20:3034–3042
33. Yang S-B, Tien A-C, Boddupalli G, Xu AW, Jan YN, Jan LY. Rapamycin ameliorates age-dependent obesity associated with increased mTOR signaling in hypothalamic POMC neurons. Neuron 2012;75:425–436
34. Vogt MC, Paeger L, Hess S, et al. Neonatal insulin action impairs hypothalamic neurocircuit formation in response to maternal high-fat feeding. Cell 2014;156:495–509
35. Schneeberger M, Gómez-Valadés AG, Altirriba J, et al. Reduced α-MSH underlies hypothalamic ER-stress-induced hepatic gluconeogenesis. Cell Rep 2015;12:361–370
36. Stevens B, Allen NJ, Vazquez LE, et al. The classical complement cascade mediates CNS synapse elimination. Cell 2007;131:1164–1178
37. Fourgeaud L, Través PG, Tufail Y, et al. TAM receptors regulate multiple features of microglial physiology. Nature 2016;532:240–244
38. Weinhard L, di Bartolomei G, Bolasco G, et al. Microglia remodel synapses by presynaptic trogocytosis and spine head filopodia induction. Nat Commun 2018;9:1228
39. Nguyen PT, Dorman LC, Pan S, et al. Microglial remodeling of the extracellular matrix promotes synapse plasticity. Cell 2020;182:388–403.e15
40. Shen K, Reichelt M, Kyauk RV, et al. Multiple sclerosis risk gene Mertk is required for microglial activation and subsequent remyelination. Cell Rep 2021;34:108835
41. Salter MW, Stevens B. Microglia emerge as central players in brain disease. Nat Med 2017;23:1018–1027
42. Jin S, Kim JG, Park JW, Koch M, Horvath TL, Lee BJ. Hypothalamic TLR2 triggers sickness behavior via a microglia-neuronal axis. Sci Rep 2016;6:29424
43. Dorfman MD, Krull JE, Scarlett JM, et al. Deletion of protein kinase c λ in POMC neurons predisposes to diet-induced obesity. Diabetes 2017;66:920–934